

Design of a Novel Aerodynamically Efficient Motorcycle

A. Sharma*, D. J. N. Limebeer#

* Department of Engineering Science
University of Oxford
Oxford, OX13PJ, United Kingdom
e-mail: amrit.sharma@eng.ox.ac.uk

Department of Engineering Science
University of Oxford
Oxford, OX13PJ, United Kingdom
e-mail: david.limebeer@eng.ox.ac.uk

ABSTRACT

Every lay person knows that two-wheeled road vehicles are potentially unstable in a capsized sense and at low speed they will simply fall over! It is less well known that these vehicles can also exhibit oscillatory instabilities, which are potentially far more dangerous. We are particularly interested in two oscillatory instabilities known as ‘wobble’ and ‘weave’. The former is reminiscent of supermarket castor shimmy, while the latter is a low frequency ‘fish-tailing’ motion that involves a combination of rolling, yawing, steering and side-slipping motions. These unwanted dynamic features, which can occur when two-wheeled vehicles are operated at speed, have been studied extensively (see [4] and the references therein). However, the authors are unable to find a reference in which these results are included in a holistic design process for a novel vehicle. This paper incorporates mathematical analysis techniques and important trends into the design process of a novel aerodynamically efficient motorcycle called the ECOSSE Spirit (ES1) [1].

A mathematical model of the ES1 is first developed using a multi-body dynamics software package called VehicleSim [2]. This high-fidelity motorcycle model includes a realistic tire-road contact geometry, a comprehensive tire model based on Magic Formulae that utilize modern tire data, tire relaxation properties and a flexible frame. Parameters describing a modern high-performance machine and rider are included. One version of the code uses VehicleSim to produce a FORTRAN or C program, which solves the nonlinear equations of motion and generates time histories, while a second version generates linearized equations of motion as a MATLAB file that contains a linearized state-space model in symbolic form. Local stability is investigated via the eigenvalues of the linearized models that are associated with equilibrium points of the nonlinear systems. The time histories produced by nonlinear simulation runs are also used to check the result.

A comprehensive study of the effects of frame flexibilities, acceleration, aerodynamics and tire variations is presented, and an optimal passive steering compensator is derived. It is shown that the traditional steering damper cannot be used to stabilize the ES1 over its entire operating regime. A simple passive compensator involving an inerter is proposed [23]. One result indicates that swinging arm flexibility can be deliberately introduced to improve the stability characteristics of the machine. However this is avoided in the final design for the ES1 with its optimal set of parameters.

Keywords: motorcycle design, motorcycle stability, aerodynamics, wobble, weave.

1 INTRODUCTION

Recently a novel motorcycle known as the ECOSSE Spirit (ES1) was designed and patented [1]. The concept vehicle features a fundamentally new chassis and steering assembly designed to have a low mass and high aerodynamic efficiency; see Figure 1.



Figure 1. Illustration (a) shows the right-side view of an aerodynamic model of the proposed vehicle; (b) shows a top view of the machine.

Computational fluid dynamics (CFD) analysis estimates the ES1’s drag-area coefficient at $0.16m^2$ – a 54% improvement over a conventional sports machine (such as the Yamaha R1), which translates into a 30% increase in top speed for any given engine power. Or alternatively, 170bhp performance with a 78bhp engine; see Figure 2. Since the initial design of the ES1 was approached from an aerodynamic perspective, the University of Oxford has been working with Spirit Motorcycle Technology on improving the overall dynamics and performance of the vehicle. This paper addresses the parameters that affect the lateral dynamics of the vehicle, which is one of the many aspects in motorcycle design.

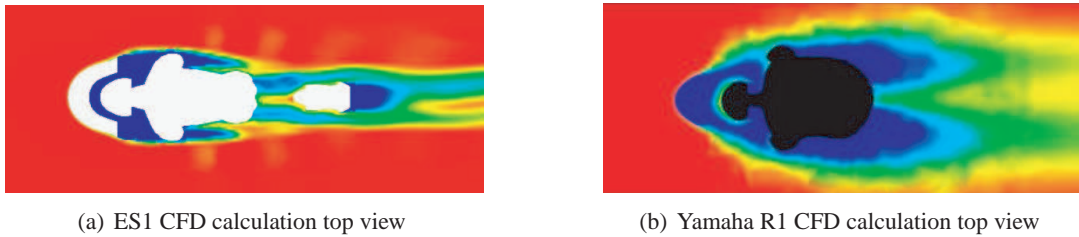


Figure 2. Plots comparing air velocity CFD calculations between the ES1 and the Yamaha R1. The ordering red-yellow-green-blue depicts the relative air velocity from low to high respectively. Plot (a) shows the air flow around the ES1-rider combination. The computed aerodynamic drag-area coefficient with the rider in the prone position is $C_dA = 0.16m^2$. Plot (b) shows the air flow around the Yamaha R1-rider combination. The computed aerodynamic drag-area coefficient with the rider in the prone position is $C_dA = 0.35m^2$.

Historically, motorcycle computer models have accurately predicted a number of real world phenomena [4]. It is therefore reasonable to first build a computer model of the ES1 and use well-known mathematical techniques, along with previous results as a guide, to identify the important parameters affecting the machine’s stability. One of the first successes of motorcycle multi-body models is [8]. The author outlined the basic features that a multi-body model requires to accurately predict a motorcycle’s lateral dynamics. Over the years models have become more complex by incorporating non-linear dynamic tire characteristics, several degrees of frame flexibility, a rider response and aerodynamics – all of which are crucial when seeking to reproduce real-world phenomena.

In Section 2 we describe the multi-body model of the ES1. This is programmed using the package VehicleSim [2], which produces both nonlinear and linearized equations of motion. Root-loci and

Nyquist diagrams of the linearized vehicle under constant speed and lean angle conditions [4], as well as acceleration and braking [5], are then used in Section 3 to determine the stability bounds on various design parameters. The vehicle parameters considered are related to the tires, the lower wishbone flexibility, the rear swinging arm flexibility, a proposed introduction of a front lateral flexibility, variations in vehicle loading, changes in the aerodynamic properties, and acceleration. The effect of each component is individually analyzed by comparing stability changes due to variations of a single parameter in an otherwise rigid vehicle. The observed trends are compared with several results in the literature [4, 10, 12], and similarities as well as differences are highlighted. Design guidelines are emphasized so that “rules of thumb” can be used when proposing the final vehicle’s parameters.

Finally, in Section 4, techniques from [3] and [7] are used to design a passive mechanical steering network that ensures stability over the machine’s velocity, roll angle and acceleration operating regimes.

2 THE MODEL

In this section we briefly introduce the multi-body model of the ES1. If further details are required then the reader is referred to [3]. The vehicle shown in Figure 1 is decomposed into the multi-body model shown Figure 3. As suggested by Figure 3, this model is based on the following kinematically interconnected rigid bodies: the main frame comprising the engine, chassis and rider, the handlebar, a link with a single translational and a single rotational degree of freedom, the small upper wishbone, the small lower wishbone, the upper wishbone, the lower wishbone, the steering body, the front wheel, the flexible swinging arm, a drive sprocket, two intermediate sprockets mounted on the swinging arm and the rear wheel. The motorcycle’s eleven constituent masses are represented by shaded circles, which are centered at their mass centers. The engine sprockets are treated as massless, but with inertia. Hinge joints with transverse axes are marked by concentric circles, and ball joints are represented by solid white circles. The parent-child relationship for each body’s coordinate system, along with the constraints, are shown in Figure 4.

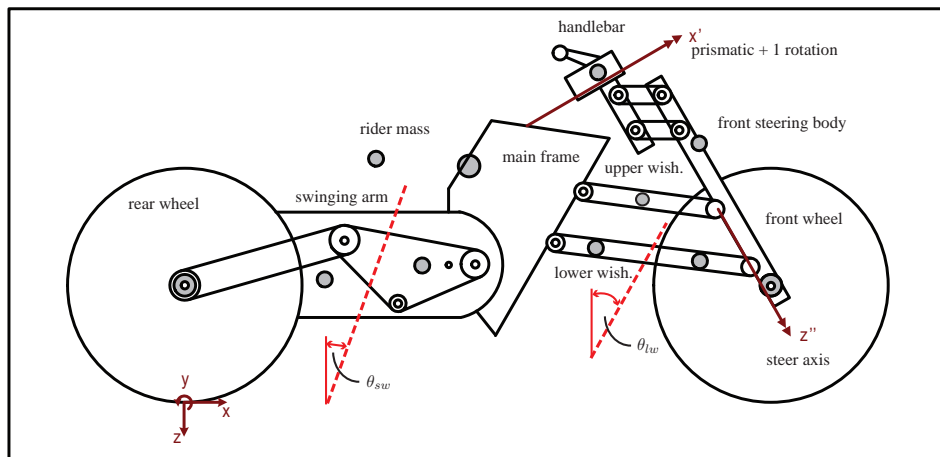


Figure 3. Diagram showing the multibody arrangement of the ES1. Shaded circles represent the body masses, white circles represent ball joints, while concentric circles show hinge joints with rotational freedoms along an axis pointing out of the page.

The rear (front) suspension is modeled via a torsional parallel spring-damper combination that act on the swinging arm (lower wishbone) and reacts on the main body. The rider is modeled as a point mass that is allowed to rotate about the main frame's body-fixed x -axis, and is restrained via a parallel spring-damper torsional compliance that acts on the rider and reacts on the main frame. The linkages between the drive and intermediate sprockets are modeled by damped elastic chains [3].

Aerodynamic influences are modeled using drag and lift forces, and a pitching moment, which are all proportional to the square of the speed. The forces are applied halfway between the wheelbase in the main frame's coordinate system.

The road tires are treated as 'wide' and flexible in compression, with two ground contact points representing the centers of the road-tire contact patches. The tire ground contact points move dynamically over the 'unspun' tire surface as the machine rolls, pitches and steers. Both tire contact points will move laterally over the tires' surface. The front tire ground contact point will also move circumferentially under combined rolling and steering. The tires' forces and moments are generated from the normal load, the tires' camber angle relative to the road and the combined slip using 'Magic Formulae' [6]. The lateral compliance of the tires' carcasses is modeled using standard linear time-varying stretched-string type tire models [6]. Relaxation effects for the longitudinal tire compliance are similarly described. In combination, the relaxation effects have a lagging influence on the generation of the tire forces and moments.

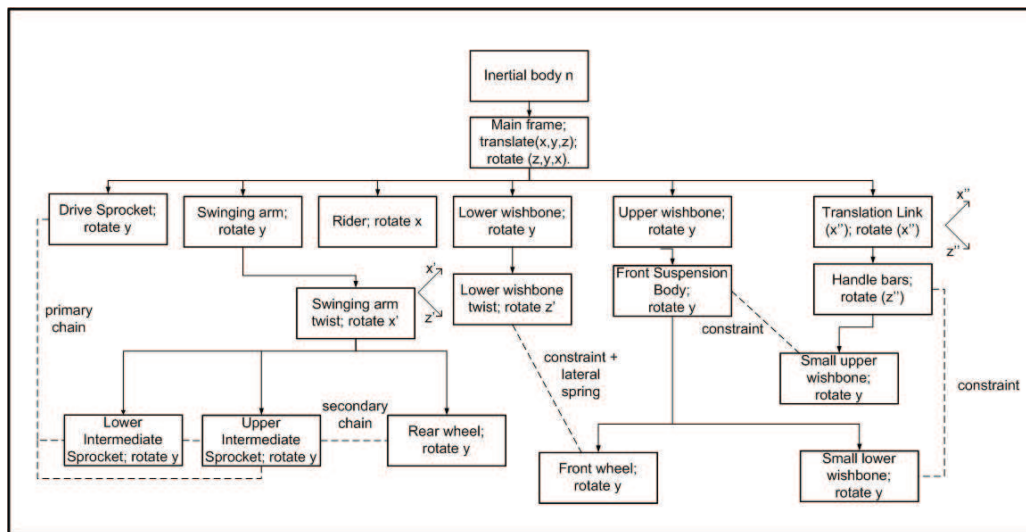


Figure 4. Parent-child tree structure of the ES1 motorcycle. The diagram shows how each body is connected and modeled in VEHICLESIM.

Inclusion of structural flexibilities in order to accurately represent the lateral dynamics of motorcycles has been studied for some time (see [10, 15, 11, 12]). These frame flexibilities turn out to be crucial in predicting the wobble oscillation frequency and damping [10, 15]. The survey paper by [4] gives a summary of the important literature related to motorcycle structural flexibility. Three frame flexibilities, modeled by parallel spring-damper arrangements, are deliberately added for the present study. These are torsional compliances in the rear swinging arm and the front lower wishbone, and a further lateral flexibility between the front wheel hub and its attachment point on the front steering body. The axes for the rear swinging arm and front lower wishbone flexibilities are in the vehicle's x - y plane and their orientations are defined by the angles θ_{sw} and θ_{lw} respectively.

The introduction of the front lateral compliance is proposed in [1] and aims to ‘mend’ cornering suspension issues, and was also studied using a simpler motorcycle model in [10].

The parent-child structure shown in Figure 4 is programmed into the multi-body modeling code VehicleSim [2], which symbolically derives the vehicle’s equations of motion. The methods used for deriving the equations of motion are based on Kane’s method [14]. The model’s state variables are the n generalized coordinates (denoted q_1, q_2, \dots, q_n) and the m generalized speeds (denoted u_1, u_2, \dots, u_m). The dimensions n and m differ when either generalized coordinates (of no interest) are omitted, or when the system is subject to nonholonomic constraints. The equations of motion are separated into the kinematic and dynamic equations. The kinematic equations are used to compute derivatives of the generalized coordinates. In matrix form, they are

$$S(\mathbf{q}, t) \dot{\mathbf{q}}(t) = \mathbf{u}(t) \quad (1)$$

in which S is an $m \times n$ matrix, \mathbf{q} is a vector containing the generalized coordinates, \mathbf{u} is a vector of generalized velocities and t is time. The dynamic equations are used to compute derivatives of the independent velocities (accelerations). In matrix form, they are:

$$M(\mathbf{q}, t) \dot{\mathbf{u}}(t) = \mathbf{f}(\mathbf{q}, \mathbf{u}, t) \quad (2)$$

where M is a $m \times m$ matrix called the mass matrix and \mathbf{f} is the force vector.

VehicleSim [2] also symbolically generates the linearized equations of motion, which we use for stability analysis. In order to compute time-invariant coefficients of the linearized equations, we require steady-state operating conditions for the nonlinear equations of motion. We do this by fitting the machine with a number of simple control systems, which in some sense mimic the rider’s control behavior. These systems control the throttle, the acceleration and braking distributions between the front and rear wheels, and the vehicle’s steering. For the purposes of the simulation model, braking is achieved with the aid of controllable braking torques that act on the front wheel and react on the front steering body. This moment represents the result of the brake friction pads coming into contact with the brake discs.

The machine’s speed is maintained using an engine drive torque that acts on the drive sprocket and reacts on the main body. In the context of the model used here the drive torque is derived from a proportional-integral controller that acts on a speed error signal. If the speed is below the reference value the drive torque is increased, while conversely, if the speed is too high the drive torque is reduced. The integral action ensures that steady-state speed errors are eliminated.

The course-following capabilities of the simulation model derive from a ‘rider’ steer torque that acts on the front steering body and reacts on the main body. The steer torque is produced by a proportional-integral-derivative feedback controller that senses a roll angle error; the PID controller’s gains are speed dependent. An expanded treatment of the vehicle modeling can be found in [3].

3 PARAMETRIC DESIGN

In modeling and designing the ES1, it is important to determine the parameters that affect stability. From the geometry of the vehicle, the lower wishbone flexibility, the rear swinging arm compliance, the tires, and the aerodynamics appear to be the key features affecting the weave and wobble modes. The effect of the experimental front lateral flexibility on the out-of-plane dynamics also requires attention. Section 3.1 argues for the use of competition racing tires. It is shown that

it is impossible to stabilize the ES1 over its entire speed range with a steering damper when the machine is fitted with typical road tires. This is because the enhanced frictional properties of competition tires improve the ES1's lateral stability. From Section 3.1 onward, the ES1 is fitted with competition tires for the remaining analyses.

Section 3.2 studies the impact on the vehicle's stability due to lateral compliance between the front wheel hub and its attachment point on the front steering body. Model A in [10] also allows the front wheel to move laterally along the wheel spindle, albeit with a simpler vehicle model. In this paper, the authors used parameters from four different production motorcycles and it is shown that the front wheel lateral compliance results in a decrease in the wobble-mode damping. This flexibility results in improved weave mode damping at moderate speeds, but worsens it for high speeds, which is where it matters. It is suggested in [10] that the lateral stiffness should be made large, but that such stiffening brings diminishing returns beyond an intermediate stiffness level. These findings are confirmed in [15]. The conclusions in [10] regarding the front lateral flexibility is corroborated by the results in Section 3.2 for the ES1 model.

The swinging arm flexibility is investigated in Section 3.3. This flexibility is also studied in [16] by augmenting the model in [17] with a rear wheel camber freedom relative to the rear frame, which is then constrained using a torsional parallel spring-damper arrangement. It is reported in [16] that the swinging arm flexibility had very little influence on the capsize and wobble modes, but it reduced the weave mode damping at medium to high speeds. Damping associated with the swinging arm flexibility made no significant difference to these findings. The results in [16] suggested that a swinging arm stiffness of $12000Nm/rad$ for a high performance machine would bring characteristics approaching that of a rigid frame. It is shown in Section 3.3 that the axis of rotation representing the swinging arm compliance is important for predicting the lateral dynamics of the ES1. It is also shown that when the ES1 is fitted with competition tires, then swinging arm compliance can be used to help stabilize the weave mode. This weave-mode trend contradicts the observations reported in [16]. However, the reader must bear in mind that very different vehicle models are being analyzed.

The effect of the lower wishbone flexibility is analyzed in Section 3.4. Literature does not exist on flexibilities of this type for motorcycles with geometries similar to that of the ES1. It is shown that there is a wobble versus weave stability compromise when introducing compliance in the lower wishbone. Moreover, the orientation of the axis of rotation for this compliance does not affect the trends observed. An argument is put forward suggesting that the lower wishbone compliance should be made as close to rigid as economically possible. This does not present a problem since product development has clearly involved substantial improvements in structural stiffness and most contemporary designs are deep into diminishing returns.

Section 3.5 focuses on how changes in the aerodynamic center of pressure, lift and pitching moments contribute to the stability properties of the ES1. The importance of aerodynamic forces on the performance and stability of motorcycles at high speeds is demonstrated in [18], which shows that the effects of aerodynamic side forces, yawing moments, and rolling moments on the lateral stability of production motorcycles are minor. As a result, we concentrate on how changes in the load distribution, due to variations in the in-plane aerodynamic forces, affect the stability of the ES1. This is important as the rider's posture can drastically alter the aerodynamic properties of the vehicle.

Using analysis techniques in [5], the effects of acceleration and braking on the wobble and weave modes are studied in Section 3.6. It is shown that the wobble mode destabilizes under braking, while the weave mode destabilizes under acceleration. These qualitative trends are consistent when

similar load transfer occurs due to aerodynamic force changes, loading variations, and constant speed uphill/downhill movements [3, 19].

3.1 The effect of competition tires

A rigid version of the ES1 model (i.e. all frame and front lateral compliances are removed) is fitted with road tires obtained from the GSXR model in [7]. A root-locus for the straight running vehicle is plotted in Figure 5 as the speed varies from 0 to $110m/s$. Modes are identified by plotting their eigenvector components, normalized with respect to the maximum component value, and checking the dominant generalized coordinates of the respective eigenvectors (see Figure 6). From Figure 5, the wobble mode is unstable at speeds above $38.4m/s$, and the weave mode is unstable at speeds greater than $88.3m/s$. As the speed increases, the wobble (weave) mode frequency decreases (increases) from $81rad/s$ ($7rad/s$) to $60rad/s$ ($32rad/s$).

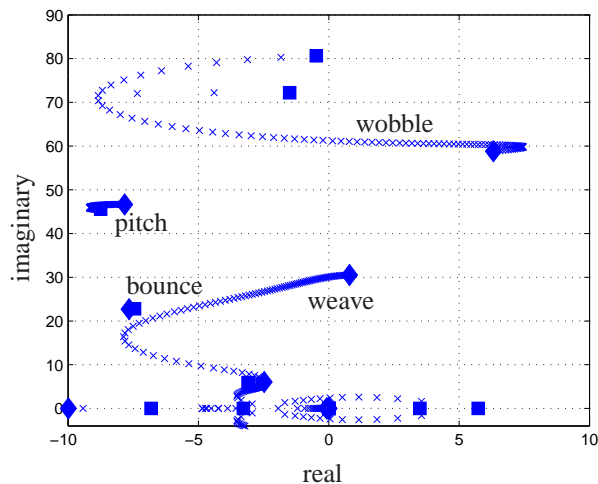


Figure 5. Straight running root-locus for the ES1 fitted with the GSXR road tires. The velocity is swept from 0 (square) to $110m/s$ (diamond). No steering damper is fitted to the vehicle.

The aim is to find a steering damper that stabilizes both the wobble and weave modes over the entire speed range. This is done by treating the ES1 as the feedback control system shown in Figure 7. Nyquist diagrams for the SISO¹ system from steering torque to steering angular velocity are plotted at two speeds: $65m/s$ (Figure 8) and $80m/s$ (Figure 9). At $65m/s$ there are two unstable complex conjugate poles associated with the wobble mode. Therefore, we require two anti-clockwise encirclements of a $-1/K$ point in the Nyquist diagram to ensure stability when using the steering damper K . In Figure 8, the leftmost intersection with the real axis, labeled A , occurs at $58.1rad/s$ (wobble frequency), and its associated real value is equal to -0.0421 . The intersection of the real axis, at -0.0104 , to the right of the wobble frequency intersection, labeled B , occurs at $25.5rad/s$ (weave frequency). Hence, the range of steering damper values to ensure stability of the ES1 fitted with road tires at $65m/s$ is $23.8Nms/rad < K < 96.2Nms/rad$.

In contrast, at $80m/s$ the problem becomes insoluble. At $80m/s$ there are two unstable complex conjugate poles that are again associated with the wobble mode. We again require two anti-

¹SISO is the acronym used for single-input single-output in the control literature.

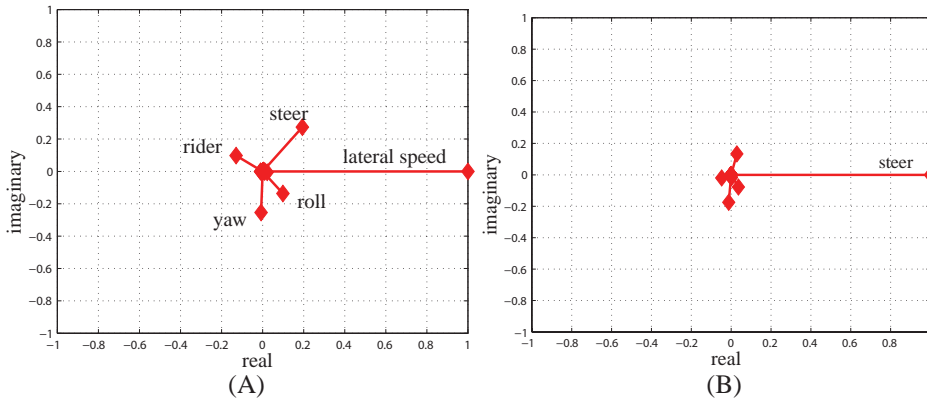


Figure 6. Plots showing the eigenvectors’ components related to generalized velocities, normalized with respect to the largest component value in each case, for the open loop weave and wobble modes of the rigid ES1 machine with a forward velocity of $60m/s$. All the states shown correspond to generalized velocities e.g. ‘steer’ is the steering’s angular velocity. Plot (A) shows the eigenvector associated with the weave mode while plot (B) is the corresponding eigenvector plot for the wobble mode.

clockwise encirclements of a $-1/K$ point in the Nyquist diagram to ensure stability when using the steering damper K . In Figure 9, the leftmost intersection with the real axis, labeled point A , occurs at $27.7rad/s$ (weave frequency) and its associated real value is -0.0433 . The intersection of the real axis to the right of the weave frequency intersection, labeled point B , occurs at $57.7rad/s$ (wobble frequency) and its corresponding real value is -0.0329 . Hence there is no steering damper that stabilizes the vehicle at $80m/s$. The maximum speed for which we can find a stabilizing steering damper is $75m/s$ (a damper of $30Nms/rad$ stabilizes the machine). Furthermore, as the steering damper increases, the wobble mode stabilizes while the weave mode destabilizes. This trend is also reported in [7] and leads to our first two design guidelines:

Design Guideline 3.1. *The open-loop system (i.e. no steering damper fitted) should be stable in weave.*

Design Guideline 3.2. *If confronted with a conflict between stabilizing wobble and stabilizing weave, opt to stabilize weave since wobble can be stabilized using a steering compensator.*

The main issue when the ES1 is fitted with the GSXR road tires is that Design Guideline 3.1 is violated. This means that in order to guarantee a stable rigid vehicle with road tires, the top speed of the ES1 must be capped to $75m/s$ and the vehicle fitted with a $30Nms/rad$ steering damper. To avoid this restriction, the tires are changed to racing slicks or competition tires. The main difference between competition racing tires and road tires is the frictional D-term of the Magic Formulae [6].

Table 1 shows that the lateral frictional forces produced by the front and rear racing tires are significantly larger than their road-tire counterparts. This increase in lateral force causes a stabilization of the weave mode at high speeds (see Figure 10). The wobble mode now enters the right-half-plane at $14.7m/s$. In obtaining a stabilizing steering damper we first calculate the root-loci for the motorcycle at different lean angles (see Figure 11). Here we confirm that Design Guideline 3.1 is satisfied and the open loop weave mode is always stable. A Nyquist diagram is plotted at the operating point that corresponds with the most unstable wobble mode: straight running at $59m/s$ (see Figure 12).

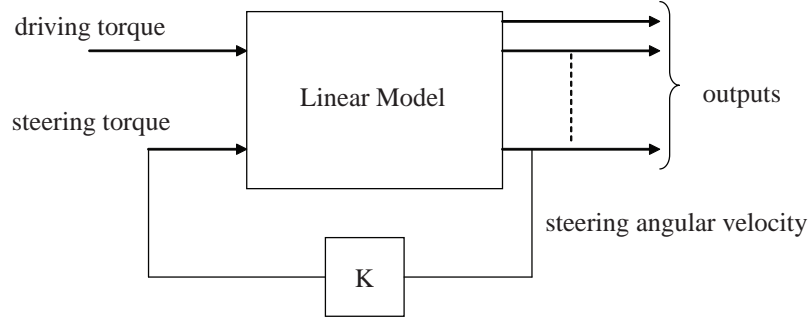


Figure 7. The feedback diagram used to design the steering damper. K is the value of the damper in Nm/rad that maps the steering angular velocity to steering torque.

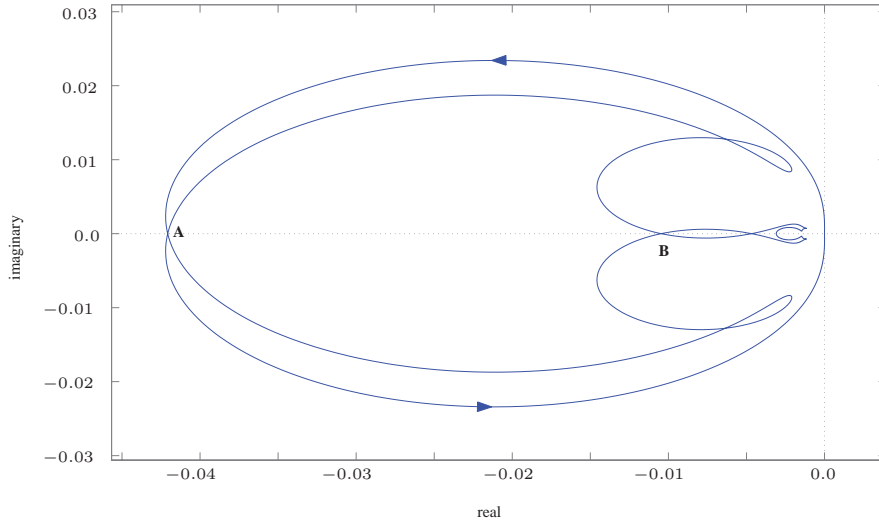


Figure 8. Nyquist diagram for the straight running ES1 fitted with the road tires found in [7]. The forward velocity is held at $65m/s$. The point labeled A occurs at an angular frequency of $58.1rad/s$ (wobble frequency) and intersects the real axis at -0.0421 . The point labeled B occurs at an angular frequency of $25.5rad/s$ (weave frequency) and intersects the real axis at -0.0104 .

| Tire | D | Road tire (N) | Racing tire (N) |
|-------|-------|-------------------|---------------------|
| Front | D_y | 1560 | 1845 |
| | D_x | 1560 | 1714 |
| Rear | D_y | 1560 | 1669 |
| | D_x | 1560 | 1543 |

Table 1. Table comparing the longitudinal and lateral frictional D -values in the Magic Formulae for the road and racing tires. The D -value associated with the lateral force is labeled D_y , while the corresponding value for the longitudinal force is labeled D_x . For both the front and rear tires, the normal force is assumed to be $1200N$.

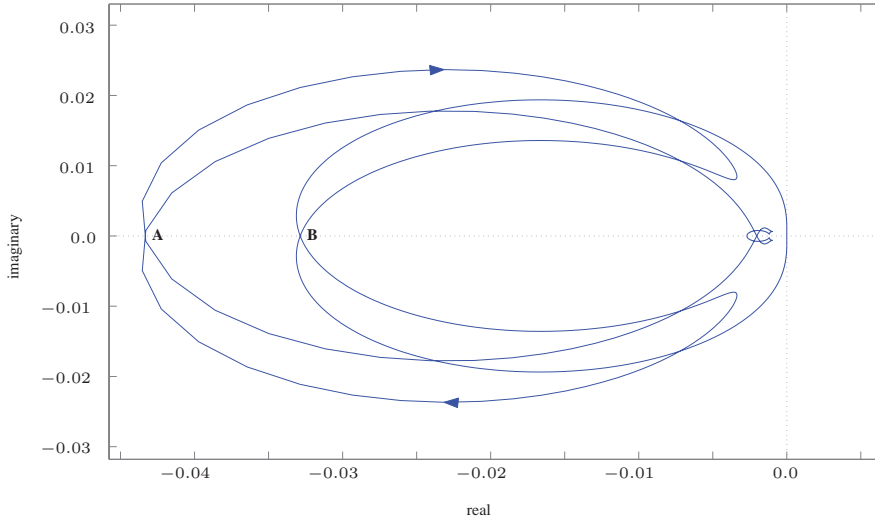


Figure 9. Nyquist diagram for the straight running ES1 fitted with the road tires found in [7]. The forward velocity is held at $80m/s$. The point labeled *A* occurs at an angular frequency of $27.7rad/s$ (weave frequency) and intersects the real axis at -0.0433 . The point labeled *B* occurs at an angular frequency of $57.7rad/s$ (wobble frequency) and intersects the real axis at -0.0329 .

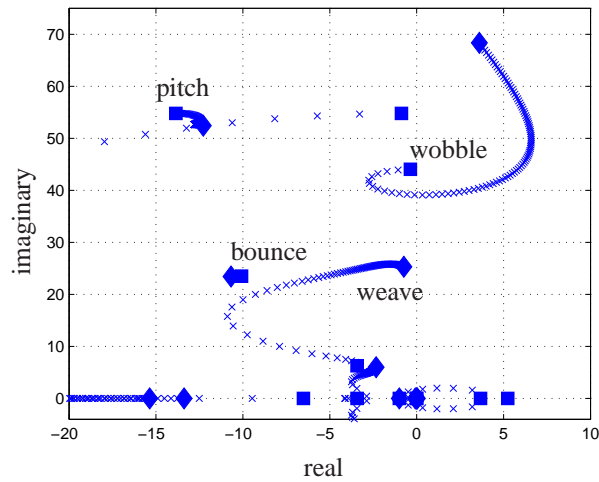


Figure 10. Straight running root-locus for the ES1 fitted with competition tires. The velocity is swept from 0 (square) to $110m/s$ (diamond). No steering damper is fitted to the vehicle.

At $59m/s$ there are two unstable complex conjugate poles that are associated with the wobble mode. Therefore in order to stabilize the vehicle, we require a damper K such that $-1/K$ lies between the points *A* and *B* in Figure 12. The point *A* corresponds to the wobble frequency $48.4rad/s$ while *B* is at the weave frequency $25.9rad/s$. Hence, a steering damper of $30Nm/rad$ stabilizes the ES1 fitted with competition tires at $59m/s$. Figure 13 shows that the $30Nm/rad$ steering damper also stabilizes the vehicle over the entire regime of operating conditions. This leads to the third design guideline:

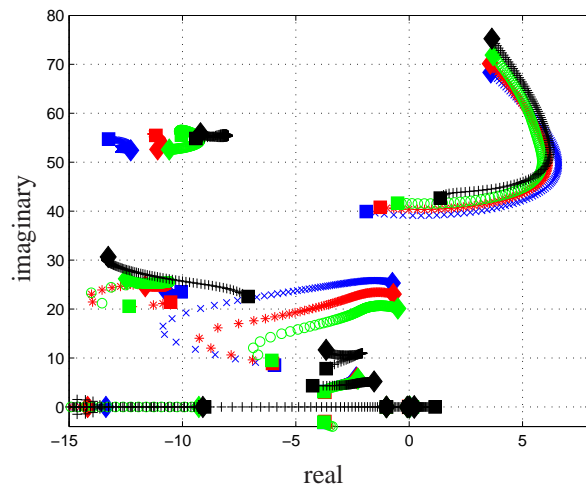


Figure 11. Root-loci for the ES1 fitted with competition tires. The velocity is swept from 10 (squares) to 110m/s (diamonds). The x-curve (blue) corresponds to a 0 degree lean, a lean of 20 degrees is shown in the *-plot (red), the o-curve (green) corresponds to 40 degrees and the +-plot (black) is 60 degrees lean. No steering damper is fitted to the vehicle.

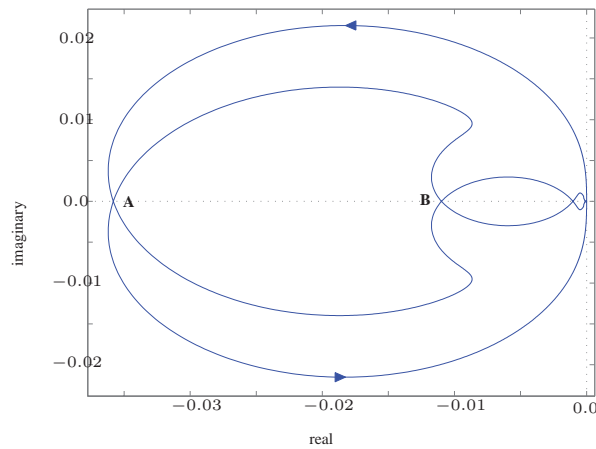


Figure 12. Nyquist diagram for competition tire model at a velocity of 59m/s. Point A corresponds to 48.4 rad/s and point B corresponds to 25.9 rad/s.

Design Guideline 3.3. *High friction tires stabilize the weave mode.*

Since we know that the ES1 fitted with competition tires is stabilizable using a steering damper, the following sections aim to isolate parameters that can be used to further ‘tweak’ the stability properties of the vehicle. This is done by using the rigid motorcycle fitted with competition tires as a benchmark when comparing the machine’s eigenvalues as a single parameter is varied.

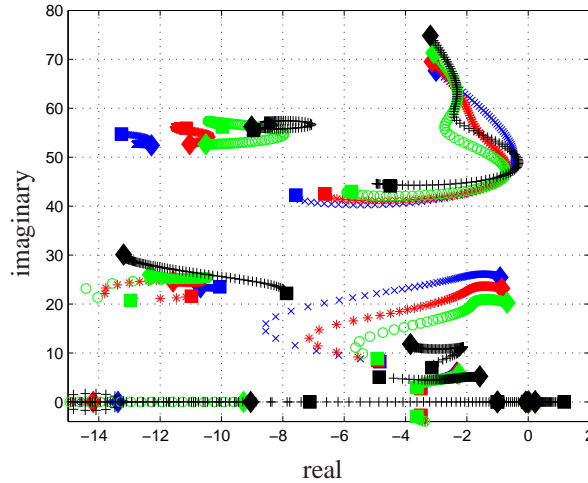


Figure 13. Root-loci for the ES1 fitted with competition tires. The velocity is swept from 10 (squares) to $110m/s$ (diamonds). The x-curve (blue) corresponds to a 0 degree lean, a lean of 20 degrees is shown in the *-plot (red), the o-curve (green) corresponds to 40 degrees and the +-plot (black) is 60 degrees lean. A steering damper of $30Nm/rad$ is fitted to the vehicle.

3.2 Proposed lateral flexibility

The diminishing effect of the suspension under cornering is a well-known issue in motorcycle dynamics. One way to potentially resolve this problem is the deliberate introduction of a damped lateral compliance between the front steering body and the lower wishbone spherical joint [1]. This section investigates the consequences on the motorcycle's stability when the proposed lateral freedom is introduced. The root-loci of the straight running vehicle when the lateral compliance stiffness and damping are $20kN/m$ and $2kNs/m$ respectively are shown in Figure 14. Two high-speed unstable modes labeled *A* and *B* are observed. The corresponding eigenvector plots in Figure 15 indicate that mode *B* is the motorcycle's weave mode, while mode *A* is a wobble-like mode that involves oscillations of the steering assembling about its roll and steer axes. What is clear from Figure 14 is that the introduction of front lateral compliance destabilizes both the weave and wobble modes.

A Nyquist diagram for the open loop system with a corresponding speed of $110m/s$ is plotted in Figure 16, and there exist no point on the real axis that the Nyquist diagram encircles four times in an anticlockwise direction. Hence, a steering damper cannot be used to stabilize the system.

To further investigate the effects of front lateral compliance, root-loci are plotted with the lateral compliance stiffness and damping as the varied parameters. The lateral compliance damping had little effect on the stability, while the lateral stiffness plays an important role. Figure 17 shows the root-loci for the straight running ES1 at $110m/s$ as the lateral stiffness compliance varies. Several conclusions are drawn from this plot. At low steering damper values, a decrease in stiffness tends to destabilize the wobble mode. Furthermore, an increase in steering damping stabilizes the wobble mode, but this has a small destabilizing effect on the weave mode. The weave mode is only stabilized at high stiffness values. As a stabilizing stiffness value is approached, the ability of the lateral stiffness to act as a suspension system under roll is clearly compromised. Thus, by applying Design Guideline 3.2, the authors advise against the deliberate introduction of a front

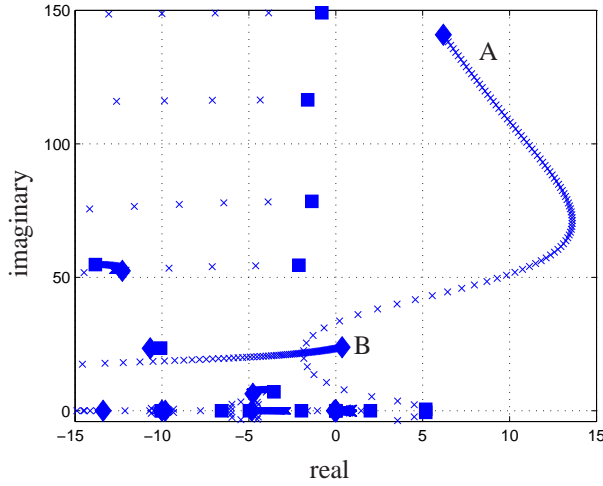


Figure 14. Root-loci for the ES1 fitted with competition tires. The stiffness and damping of the lateral steering compliance are $20kN/m$ and $2kNs/m$ respectively. No steering damper is fitted to the vehicle and the velocity is swept from 0 (square) to $110m/s$ (diamond). Mode B crosses into the right-half-plane at $98.1m/s$ while mode A intersects the imaginary axis at $5.5m/s$ and $14.5m/s$.

lateral compliance. This conclusion is corroborated by [10].

3.3 Rear swinging arm flexibility

The effect of a rear swinging arm flexibility along the body-fixed z -axis is shown in Figure 18. Figure 18 (A) holds the compliance damping at $50Nms/rad$ and varies the lower wishbone stiffness from $1kNm/rad$ to $500kNm/rad$. Figure 18 (B) holds the flexibility stiffness at $10kNm/rad$ and varies its damping from $5Nms/rad$ to $500Nms/rad$. Interestingly, these plots indicate that the rear swinging arm flexibility stabilizes both the weave and the wobble modes. However, introducing swinging arm flexibility brings a swinging arm flexing mode into consideration. Even though the swinging arm flexing mode is stabilized at intermediate stiffness and damping values, it is ill-advised to deliberately introduce a potentially unstable mode. Compliance damping heavily affects the wobble mode while having little effect on the weave mode.

Another interesting observation is the change in the characteristics of the root-locus when the swinging arm deflection axis is rotated 90 degrees to lie along the beam's x -axis (see Figure 19). This type of flexibility stabilizes the weave mode while having almost no effect on the wobble mode. From the trends obtained in these plots, it is concluded that a controlled introduction of swinging arm flexibility can be used to improve the stability properties of the vehicle. However, there is an issue in trying to independently introduce torsional flexibility along two orthogonal axes of the beam. A hypothetical model is presented in the final design chapter of [3] that deliberately uses torsional flexibility of the rear swinging arm to help improve the stability of the weave mode. Whether this can be manufactured in practice is an issue beyond the scope of the present analysis. To avoid this issue the ES1's swinging arm is made as stiff as economically possible ($> 11kNm/rad$).

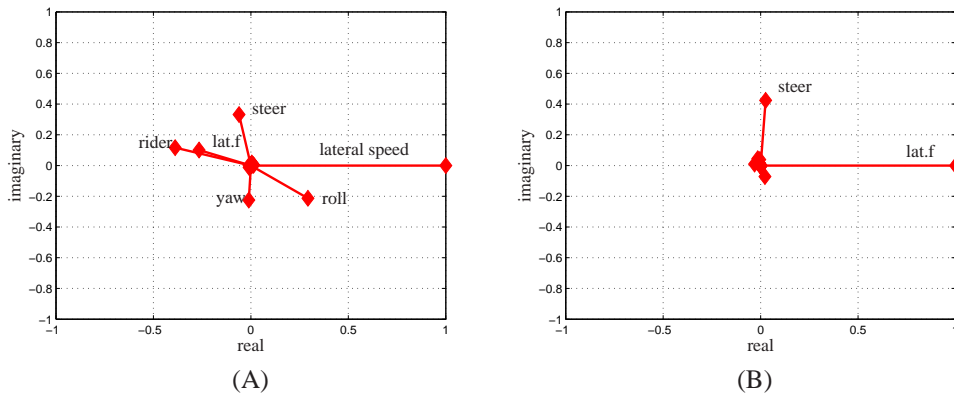


Figure 15. Plots showing the eigenvectors' components related to generalized velocities, normalized with respect to the largest component value in each case, for the ES1 machine described in Figure 14 with a forward velocity of $100m/s$. Plot (A) shows the eigenvector associated with the weave-like mode labeled *B* in Figure 14. This mode contains the generalized coordinates of a typical weave mode along with the compliance deflection term. Plot (B) shows the eigenvector associated with the wobble-like mode labeled *A* in Figure 14. This mode involves the steering assembly oscillating about both its steer and roll axes.

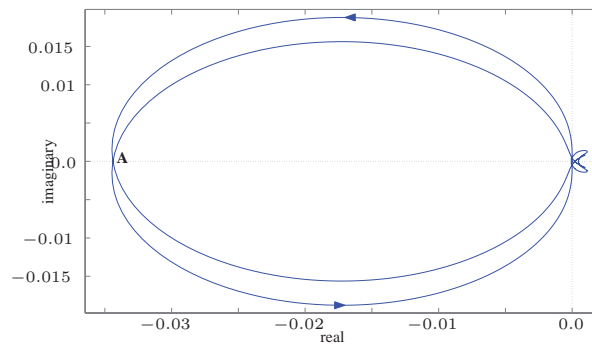


Figure 16. Nyquist diagram for the ES1 fitted with competition tires. The stiffness and damping of the lateral steering compliance are $20kN/m$ and $2kNs/m$ respectively. The diagram corresponds to the operating point of the straight running vehicle with velocity of $110m/s$. Point *A* corresponds to the wobble-like mode's frequency of $141rad/s$.

3.4 Front lower-wishbone flexibility

The effect of a front lower wishbone flexibility along the body's z -axis is shown in Figure 20. Figure 20 (A) holds the compliance damping at $50Nms/rad$ and varies the lower wishbone stiffness from $1kNm/rad$ to $500kNm/rad$. The lower wishbone stiffness is held at $10kNm/rad$ in Figure 20 (B) and its damping varies from $5Nms/rad$ to $500Nms/rad$. These plots demonstrate that a flexible lower wishbone destabilizes the weave mode while stabilizing the wobble mode. The lower wishbone flexibility has a greater influence in affecting the wobble mode than the weave mode. This trend remains unchanged when the deflection axis is rotated 90 degrees and is oriented parallel to the beam's x -axis (see Figure 21). Using Design Guideline 3.1 and Design Guideline 3.2, the lower wishbone flexibility should be made large, but such stiffening

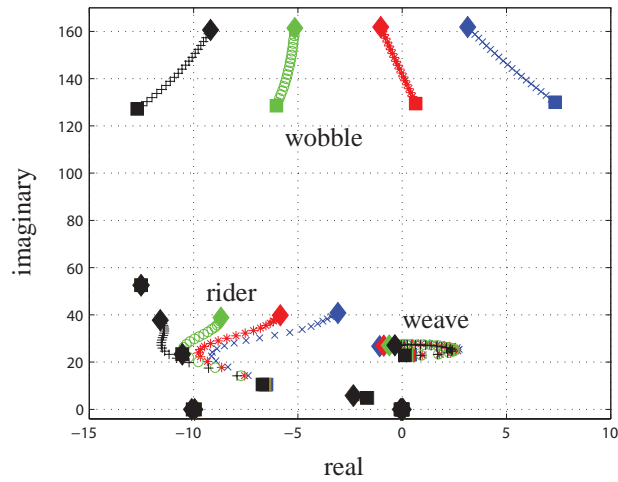


Figure 17. Root-loci for the ES1 fitted with competition tires as the lateral compliance stiffness varies from $1kN/m$ (square) to $500kN/m$ (diamond). The lateral compliance damping and the vehicle's velocity are fixed at $2kNs/m$ and $100m/s$ respectively. The x-curve (blue), *-curve (red), o-curve (green) and +-curve (black) correspond to steering dampers of 0, 30, 60 and $90Nm/s/rad$ respectively. The weave mode stabilizes in the x-curve (blue), *-curve (red), o-curve (green) and +-curve (black) at stiffness values of 320, 350, 385 and $430kN/m$ respectively.

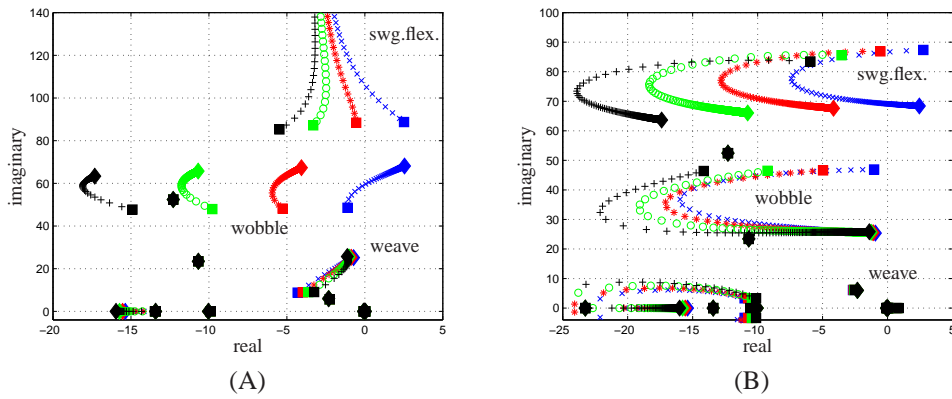


Figure 18. Plots (A) and (B) correspond to a swinging arm flexibility compliance about the wishbone's body-fixed z -axis. The ES1 is fitted with competition tires and the plots correspond to a forward velocity of $110m/s$. The x-curve (blue), *-curve (red), o-curve (green) and +-curve (black) correspond to steering dampers of 0, 30, 60 and $90Nm/s/rad$ respectively. Plot (A) is the root-locus when the torsional damping is held at $50Nm/s/rad$ while the stiffness is swept from $1kNm/rad$ (square) to $500kNm/rad$ (diamond). Plot (B) is the root-locus when the torsional stiffness is held at $10kNm/rad$ while the torsional damping is swept from 5 (square) to $500Nm/s/rad$ (diamond).

brings diminishing returns beyond an intermediate stiffness value. From the root-loci calculations, the improvement in the weave mode is minimal when further stiffening the beam beyond

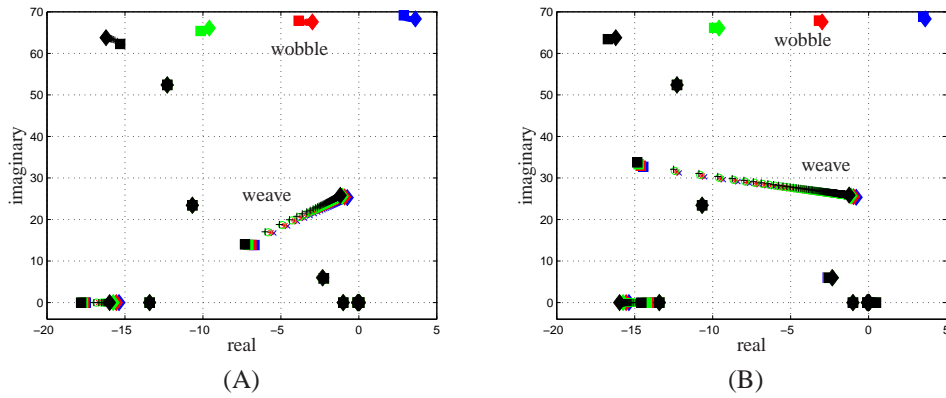


Figure 19. Plots (A) and (B) correspond to a swinging arm flexibility compliance about the wishbone's body-fixed x -axis. The ES1 is fitted with competition tires and the plots correspond to a forward velocity of $110m/s$. The x -curve (blue), $*$ -curve (red), o -curve (green) and $+$ -curve (black) correspond to steering dampers of 0, 30, 60 and $90Nm/s/rad$ respectively. Plot (A) is the root-locus when the torsional damping is held at $50Nm/s/rad$ while the stiffness is swept from $1kNm/rad$ (square) to $500kNm/rad$ (diamond). Plot (B) is the root-locus when the torsional stiffness is held at $10kNm/rad$ while the torsional damping is swept from 5 (square) to $500Nm/s/rad$ (diamond).

$12-13kNm/rad$. Numerical studies indicate that the front lower wishbone stiffness should exceed $> 12kNm/rad$.

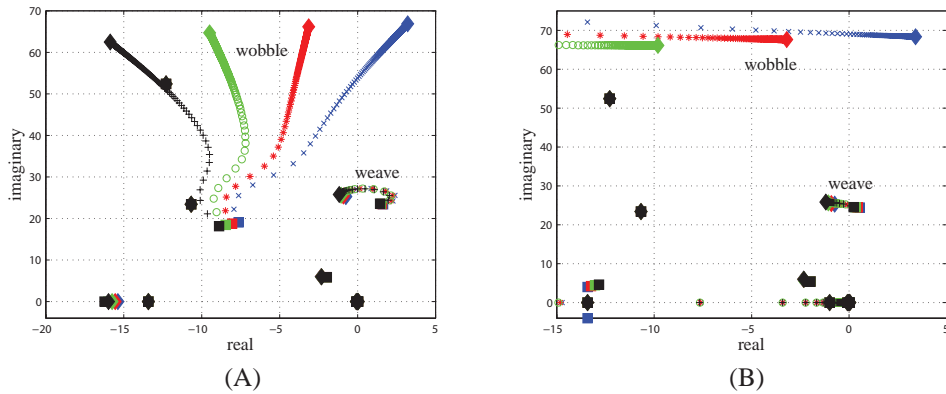


Figure 20. Plots (A) and (B) correspond to a lower wishbone flexibility compliance about the wishbone's body-fixed z -axis. The ES1 is fitted with competition tires and the plots correspond to a forward velocity of $110m/s$. The x -curve (blue), $*$ -curve (red), o -curve (green) and $+$ -curve (black) correspond to steering dampers of 0, 30, 60 and $90Nm/s/rad$ respectively. Plot (A) is the root-locus when the torsional damping is held at $50Nm/s/rad$ while the stiffness is swept from $1kNm/rad$ (square) to $500kNm/rad$ (diamond). The weave mode crosses the imaginary axis at approximately $12kNm/rad$. Plot (B) is the root-locus when the torsional stiffness is held at $10kNm/rad$ while the torsional damping is swept from 5 (square) to $500Nm/s/rad$ (diamond). The weave mode crosses crosses the imaginary axis at $300Nm/s/rad$.

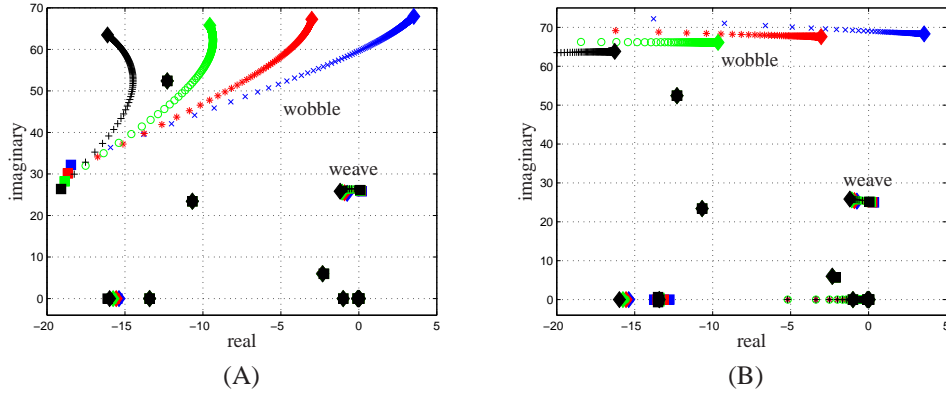


Figure 21. Plots (A) and (B) correspond to a lower wishbone flexibility compliance about the wishbone’s body-fixed x -axis. The ES1 is fitted with competition tires and the plots correspond to a forward velocity of $110m/s$. The x -curve (blue), $*$ -curve (red), o -curve (green) and $+$ -curve (black) correspond to steering dampers of 0, 30, 60 and $90Nm/s/rad$ respectively. Plot (A) is the root-locus when the torsional damping is held at $50Nm/s/rad$ while the stiffness is swept from $1kNm/rad$ (square) to $500kNm/rad$ (diamond). Plot (B) is the root-locus when the torsional stiffness is held at $10kNm/rad$ while the torsional damping is swept from 5 (square) to $500Nm/s/rad$ (diamond).

The conclusions in Sections 3.2, 3.3 and 3.4 lead to the fourth design rule:

Design Guideline 3.4. *The motorcycle’s frame should be made as stiff as economically possible.*

3.5 Aerodynamics and vehicle loading

The effect of moving the aerodynamic center of pressure, changing the load distribution and increasing the aerodynamic pitching moment are all related. These effects also occur in many practical situations e.g. the rider sitting upright on the ES1 or loading the rear of the vehicle. It is therefore important to determine the changes in the ES1’s stability properties as a pitching moment is applied. A root-locus, with a pitching moment as the varied parameter, is plotted at the operating point that corresponds with the most unstable wobble mode: straight running at $59m/s$ (see Figure 22). The pitching moment is increased from 0 to $700Nm$ —this corresponds to halving the load at the front wheel. The results show a stabilization in the wobble mode and a possible destabilization in the weave mode. The choice of steering damper dictates the trend in the weave mode as the pitching moment is increased. However, the system remains stable for a moderate steering damper value.

3.6 Acceleration and braking

In order to use the method derived in [5] to study stability changes due to acceleration, a bound on the maximum accelerating force must be obtained. The range of inertial forces that the vehicle undergoes is calculated in [3], where the maximum acceleration/braking force is limited by the machine’s tires. The ES1’s maximum acceleration and deceleration plotted as a function of velocity is shown Figure 23 (see [3] for details). Knowing that a velocity of $59m/s$ corresponds to the most unstable wobble mode while $100m/s$ is associated with the least stable weave mode, two acceleration ranges are considered. The first, shown in Figure 24 (A), investigates the stability of the vehicle at a speed of $59m/s$ under accelerations from 0 to $7m/s^2$ and decelerations from

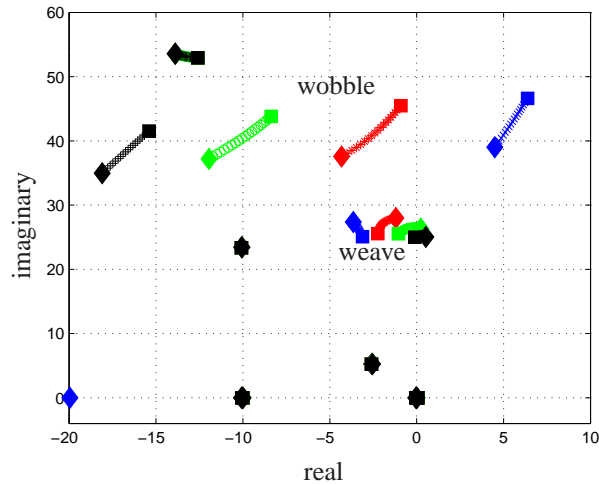


Figure 22. Root-loci for the straight running ES1 fitted with competition tires as the aerodynamic pitching moment is increased from 0 (square) to $700Nm$ (diamond). The machine's forward velocity is held at $59m/s$. The x-curve (blue), *-curve (red), o-curve (green) and +-curve (black) correspond to steering dampers of 0, 30, 60 and $90Nm/s/rad$ respectively.

0 to $13m/s^2$. The second, shown in Figure 24 (B), looks at the stability of the ES1 at a speed of $100m/s$ under accelerations from 0 to $3.8m/s^2$ and decelerations from 0 to $15.8m/s^2$.

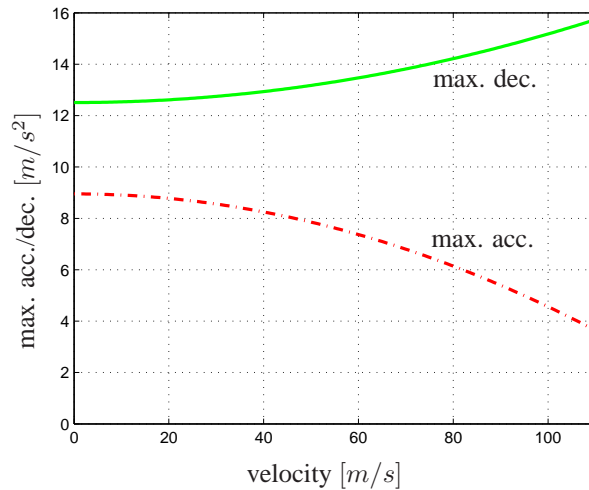


Figure 23. Plot for the ES1 fitted with competition tires showing the maximum acceleration and deceleration values as a function of its traveling velocity. The solid (green) curve corresponding to the maximum deceleration value while the dashed (red) plot is the maximum acceleration. The plots are generated using equations in Section 7.6 in [3].

In Figure 24 (A), the weave mode corresponding to 40 degrees lean crosses the imaginary axis at $6.9m/s^2$ and the wobble mode for the straight running vehicle goes unstable at $-4.6m/s^2$. Here we conclude that under straight running conditions, acceleration has a destabilizing (stabilizing)

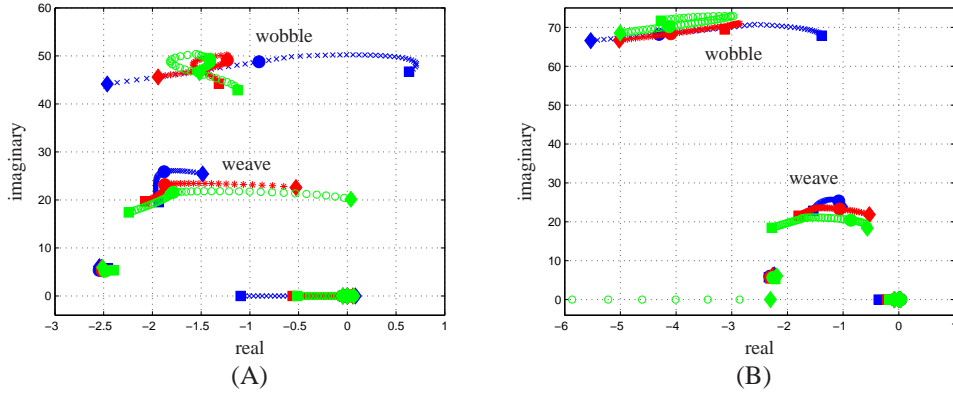


Figure 24. Root-loci for the ES1 fitted with competition tires and a steering damper of 30Nm/s/rad as acceleration is varied. The eigenvalues correspond to roll angles of 0 degrees (blue x-curve), 20 degrees (red *-curve) and 40 degrees (green o-curve). The solid circle on each curve corresponds to the zero acceleration point. Plot (A) corresponds to the vehicle’s velocity being held at 59m/s as the acceleration inertial forces are varied from -13m/s^2 (square) to 7m/s^2 (diamond). Plot (B) corresponds to the vehicle’s velocity being held at 100m/s as the acceleration inertial forces are varied from -15.8m/s^2 (square) to 3.8m/s^2 (diamond).

effect on the weave (wobble) mode while deceleration has a destabilizing (stabilizing) effect on the wobble (weave) mode. The weave mode trend tends to remain the same under cornering while the wobble mode becomes less sensitive to acceleration under lean. In designing a steering damper, it is crucially important to consider changes in the wobble and weave mode stability properties under acceleration. This is especially the case at intermediate speeds like 59m/s . At higher speeds, like 100m/s (see Figure 24 (B)), both the wobble and weave modes remain stable across the range of possible accelerations. Here the trends are consistent with those observed at intermediate speeds.

The problem of an unstable weave mode under high lean and acceleration, and an unstable wobble mode under zero lean and deceleration, poses a complex stabilization problem (Design Guideline 3.1 is violated). This is because there is no steering damper that can simultaneously stabilize both the wobble and weave modes. A similar result is shown for the GSXR1000 motorcycle studied in [20]. The simultaneous stabilization of both the wobble and weave modes is solved by optimizing the vehicle fitted with a more general steering compensator.

The conclusions in Sections 3.5 and 3.6 lead to the final rule-of-thumb:

Design Guideline 3.5. *Load transferred onto the rear (front) wheel destabilizes weave (wobble).*

4 STEERING COMPENSATOR DESIGN

Assuming that we don’t cap the top speed of the ES1, then a more general steering compensator is needed in place of the steering damper. This means that instead of the constant feedback gain K in Figure 7, we design a stabilizing transfer function $K(s)$. If we place passivity restrictions on $K(s)$, then the compensator can be synthesized using springs, dampers and inerters [21, 22, 23]. We seek the simplest passive mechanical network that stabilizes the rigid vehicle fitted with competition tires over the motorcycle’s operating envelope.

The operating envelope consists of two groups of linearized models that ‘grid’ the machine’s operating regime. The first group involves the vehicle’s behavior from low ($10m/s$) to medium ($70m/s$) speeds, over lean angles from 0 to 40 degrees and accelerations from $-10m/s^2$ to $7m/s^2$. The second group involves the vehicle’s behavior from low ($10m/s$) to high speeds ($100m/s$), over lean angles from 0 to 40 degrees and accelerations from $-13m/s^2$ to $3m/s^2$. The motivation behind this comes from the trend that the real part of the wobble (weave) mode is maximized at medium (high) speeds and that the acceleration envelope is a function of speed. The idea is to capture the most unstable modes of the ES1 by considering both medium and high accelerations with their corresponding velocity ranges. When forming the grid, velocities are incremented by $0.1m/s$, accelerations by $1m/s^2$ and roll angles by 5 degrees.

The main ingredients of the network design problem are: (i) the weave mode is stable in the open loop, while the wobble unstable; (ii) any attempt to stabilize the wobble mode with steering damping, destabilizes the weave mode (Design Guideline 3.2); and (iii) the frequency separation between wobble ($58.1rad/s$) and weave ($25.5rad/s$) is approximately $33rad/s$. It is therefore reasonable to implement a high-pass filter as the steering compensator. The simplest high pass filter is an inerter, b , in series with a damper, c . This gives a high frequency gain equal to the damping value c and a break frequency of c/b .

As a preliminary design, the break frequency is placed at $30rad/s$ and the high frequency gain is set as 30. Using this as a starting point, an optimization procedure that minimizes the largest damping ratio, between wobble and weave, is carried out over the machine’s operating envelope; see Chapter 9 of [3] for details or [7] for the general optimization procedure. A $27.3Nms/rad$ steering damper in series with a $0.78kg.m^2$ inerter is calculated as the optimal network parameters. The introduction of phase lead ensures that the weave and wobble modes are stable over the machine’s entire operating regime.

5 CONCLUSIONS

General trends are outlined relating the ES1’s stability with various parameters. Design guidelines and suggestions are presented that can be extended to general motorcycle design. It is shown in Section 3.1, that the high lateral frictional coefficient of racing slick tires is needed to help stabilize the weave mode at high speeds. The avoidance of a deliberate introduction of front lateral compliance is advised in Section 3.2 due to its destabilizing effect on the weave mode. There seems to be no advantage in allowing a lower wishbone flexibility. This should be made stiff enough so that the beam behaves as a rigid object in the dynamic analysis. Substantial stiffening of the lower wishbone should not present a practical problem as most contemporary designs are deep into diminishing returns for additional stiffness. Introducing swinging arm flexibility can improve the stability properties of the vehicle. The torsional axis of the swinging arm flexibility is important when predicting the vehicle’s stability properties at low stiffness values. Theoretically, a low torsional stiffness about an axis parallel to the beam’s x -axis helps stabilize the weave mode, while having little impact on the wobble and swinging arm flexing modes. It is suggested that this property can be used to experimentally improve the stability properties of the ES1.

Changes in the aerodynamic center of pressure and variational loading of the vehicle are also analyzed. Here the emerging trend is a stabilization of the wobble mode as front wheel loading decreases and, depending on the vehicle’s steering damper, a possible destabilization of the weave mode as rear wheel loading increases. This trend also emerged in the acceleration study of Section 3.6.

The study of the vehicle under acceleration (braking) first approximated the range of accelerations (decelerations) the ES1 can undergo at a specific velocity. This is used to study the lateral stability of the vehicle under acceleration (braking) at intermediate and high speeds. The results show that inertial forces are crucial when designing a steering compensator for the ES1. Under straight running conditions, acceleration has a destabilizing (stabilizing) effect on the weave (wobble) mode while deceleration has a destabilizing (stabilizing) effect on the wobble (weave) mode. The weave mode trends tend to remain the same under cornering while the wobble mode becomes less sensitive to acceleration under lean. We conclude that no damper exists that can simultaneously stabilize the ES1 over its entire operating regime. Provided that the top speed of the machine is not limited, the stabilization problem is solved by using a steering compensator consisting of an inerter in series with a damper.

REFERENCES

- [1] R. Glover, "Improvements in or relating to motorcycles", *Patent for Spirit Motorcycle Technology Limited*, 2006.
- [2] Anon., "VehicleSim Lisp Reference Manual Version 1.0", *Mechanical Simulation Corporation*, <http://www.carsim.com>, 2008.
- [3] A. Sharma, "Stability Analysis of Bicycles and Motorcycles", *PhD Thesis*, Imperial College London, 2010.
- [4] D. J. N. Limebeer and R. S. Sharp, "Bicycles, Motorcycles and Models", *IEEE Control Systems Magazine*, **26(5)** (2006), pp. 34–61.
- [5] D. J. N. Limebeer and A. Sharma, "Burst oscillations in the accelerating bicycle", *Journal of Applied Mechanics*, Accepted 2010.
- [6] H. B. Pacejka, *Tyre and Vehicle Dynamics*, Butterworth and Heinemann, Oxford, 2002.
- [7] S. Evangelou, D. J. N. Limebeer, R. S. Sharp and M. C. Smith, "Steering compensators for high-performance motorcycles", *ASME Journal of Applied Mechanics*, **74(5)** (2007), pp. 332–346.
- [8] R. S. Sharp, "The stability and control of motorcycles", *Jour. Mech. Eng. Sci.*, **13(5)** (1971), pp. 316–329.
- [9] R. S. Sharp, "A review of motorcycle steering behaviour and straight line stability characteristics", *Society of Automotive Engineers*, **780303** (1978).
- [10] R. S. Sharp and C.J. Alstead, *The influence of structural flexibilities on the straight running stability of motorcycles*, *Vehicle system dynamics*, **9** (1980), pp. 327–357.
- [11] C. G. Giles and R. S. Sharp, "Static and dynamic stiffness and deflection mode measurements on a motorcycle, with particular reference to steering behaviour", *Proc. Inst. Mech. Eng./MIRA Conference on Road Vehicle Handling*, Mechanical Engineering Publications, 1983, pp. 185–192.
- [12] R. S. Sharp, "Vibrational modes of motorcycles and their design parameter sensitivities", *Vehicle NVH and Refinement, Proc Int Conf.*, Mech. Eng. Publications, Birmingham 3–5 May 1994, pp. 107–121.

- [13] F. Biral, D. Bortoluzzi, V. Cossalter and M. Da Lio, “Experimental study of motorcycle transfer functions for evaluating handling”, *Vehicle System Dynamics*, **39(1)** (2003), pp. 1–26.
- [14] M. Sayers, “Symbolic vector/dyadic multibody formalism for tree-topology systems”, *Journal of Guidance, Control, and Dynamics*, **14(6)** (1991), pp. 1240–1250.
- [15] P. T. J. Spierings, “The effects of lateral front fork flexibility on the vibrational modes of straight-running single-track vehicles”, *Vehicle System Dynamics*, **10(1)** (1981), pp. 21–35.
- [16] R. S. Sharp, “The influence of frame flexibility on the lateral stability of motorcycles”, *Journal of Mechanical Engineering Science*, **16** (1974), pp. 117–120.
- [17] R. S. Sharp, “The stability and control of motorcycles”, *Jour. Mech. Eng. Sci.*, **13(5)** (1971), pp. 316–329.
- [18] K. R. Cooper, “The effects of aerodynamics on the performance and stability of high speed motorcycles”, *Proc. 2nd AIAA Symp. Aerodynamics Sport Competition Automobiles*, **2** (1974).
- [19] D. J. N. Limebeer, R. S. Sharp and S. Evangelou, “The stability of motorcycles under acceleration and braking”, *Jour. Mech. Eng. Sci.*, **215(9)** (2001), pp. 1095–1109.
- [20] A. Sharma, “Analysis, design and optimization of motorcycle steering compensators under constant acceleration and deceleration”, *MEng. Report, Imperial College London*, (2006).
- [21] O. Brune, “Synthesis of finite two terminal network whose driving point impedance is a prescribed function of frequency”, *Journal of Mathematical Physics*, **10** (1931).
- [22] R. Bott and R. J. Duffin, “Impedance synthesis without use of transformers”, *Journal of Applied Physics*, **20** (1949).
- [23] M. C. Smith, “Synthesis of mechanical networks: the inerter”, *IEEE transactions on automatic control*, **47** (2002), pp. 1648-1662.